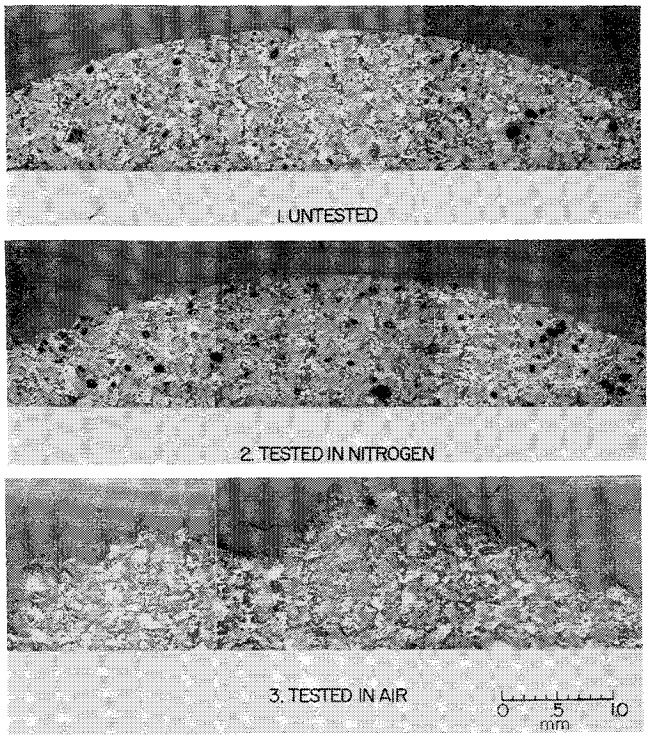

Fig. 3 Comparison of photomicrographic sections of graphite specimens.

the binder matrix to occur before filler grains can be readily removed by external forces.

Mechanisms of Binder Weakening

A number of mechanisms can be proposed to account for the weakening of the binder matrix. Which mechanisms are operative or predominate in any situation will depend considerably on the temperature, pressure, and flow velocity of the environment. Among the possible mechanisms are reaction of the gaseous reactant with the binder in the pores due to penetration of the reactant into the pore structure,[1] higher recession rate of the binder because of its lower density than the filler,[5] thermal stress cracking of the binder due to severe temperature gradients, sublimation of the binder bridges within the pore structure,[5] and preferential sublimation of the binder compared with the filler.

One potentially important mechanism, which may not be as apparent as those already mentioned, perhaps warrants some discussion. This mechanism is based on the assumption that the binder phase in graphite is inherently more reactive than the filler phase. That is, at a given temperature and concentration of oxygen, the binder will oxidize faster than the filler. Preferential oxidation of the binder has been suggested before[4,6] and the assumption seems to be well founded. Based on this assumption it is obvious that at temperatures at which the reaction rate is controlled by chemical kinetics, the binder will recede faster than the filler. It is not as obvious, however, that preferential recession of the binder can occur even at higher temperatures at which the reaction rate is diffusion controlled.

For diffusion controlled reactions, the observed reaction rate is limited by the rate of diffusion of oxygen to the reacting surface and, thus, chemical kinetics can often conveniently be disregarded. However, at the reacting surface the reaction proceeds according to conventional kinetic laws provided, of course, that the oxygen concentration considered is the concentration immediately adjacent to the surface (as opposed to the freestream concentration). It is obvious that this oxygen concentration, although small, must be nonzero, otherwise no chemical reaction could proceed. (In practice, this concentration generally cannot be measured, which is, of course, one reason why the concept of diffusion control is utilized.) However, whatever the oxygen concentration, and in whatever manner it may vary over the surface, it cannot vary discontinuously. Accordingly, at an interface between two adjacent solid phases, both phases will see the same concentration. But, as stated previously, whenever two phases with different reactivity see the same concentration the more reactive phase will oxidize faster. Thus, in the case of graphite, at each interface between binder and filler, the binder will recede faster and thereby expose the filler grains making them more vulnerable to mechanical and aerodynamic forces.

Conclusions

Direct experimental evidence obtained with high-speed motion pictures demonstrates that mechanical or aerodynamic removal of incompletely oxidized particulate matter contributes to the total ablative mass loss of polycrystalline, artificial graphite in dynamic, oxidizing environments. This removal is facilitated by the weakening of the binder matrix by oxidation. A mechanism for this weakening, based on the greater oxidative reactivity of binder than filler, is proposed. This mechanism should be effective in diffusion controlled environments as well as in kinetically controlled environments.

References

[1] Gulbransen, E. A., Andrew, K. F., and Brassart, F. A., "Ablation of Graphite in Oxygen and Air at 1000–1400°C Under Flow Conditions," *Carbon*, Vol. 1, 1964, pp. 413–424.

[2] Khanin, M. V., "Mechanism of Destruction of Polycrystalline Graphite by Erosion," *Soviet Physics—Technical Physics*, Vol. 11, No. 6, Dec. 1966, pp. 540–543.

[3] Maahs, H. G. and Schryer, D. R., "Chemical Impurity Data on Selected Artificial Graphites with Comments on the Catalytic Effect of Impurities on Oxidation Rate," TN D-4212, Oct. 1967, NASA.

[4] Maahs, H. G., "Crystallographic Data on Selected Artificial Graphites with Comments on the Role of the Degree of Crystal Development in Oxidation," TN D-4888, Nov. 1968, NASA.

[5] Kratsch, K. M. et al., "Graphite Ablation in High-Pressure Environments," AIAA Paper 68-1153, Williamsburg, Va., 1968.

[6] Riley, W. C., "Graphite," *High-Temperature Materials and Technology*, edited by I. E. Campbell and E. M. Sherwood, Wiley, New York, 1967, Chap. 7, pp. 188–234.

Lift Effectiveness of Slender Wings with Streamwise Root Gaps and Fences

M. Judd*
University of Southampton, Southampton, England

Introduction

THE presence of a streamwise root gap has a large effect on the lift effectiveness of slender wings which has been explained[1,2] on the basis of slender wing theory. One application is to the case of missile configurations equipped with all-moving low aspect ratio control surfaces. However, a similar effect is present[3] in wind-tunnel measurements made on slender half-models using the tunnel wall as a plane of symmetry. This is particularly relevant to dynamic testing where a streamwise root gap is required for mechanical

Received June 9, 1969; revision received July 29, 1969.

* Lecturer, Department of Aeronautics and Astronautics; now Visiting Associate Professor, Department of Aeronautics and Astronautics, Massachusetts Institute of Technology, Cambridge, Mass.

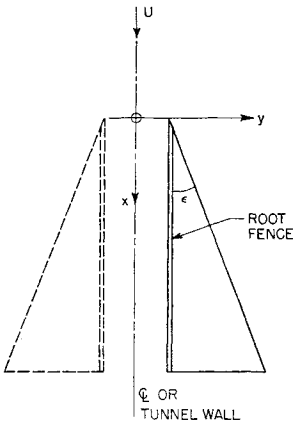

Fig. 1 Wing plan form and coordinate system.

clearance. It has been shown[3] that all the stability derivatives are affected grossly and similarly by the gap.

A practical solution sometimes adopted in this situation is to attach a small fin plate or "fence" along the root. The purpose of the present work is to put this on a theoretical basis, to investigate the root fence effectiveness, and to indicate how a minimum size might be chosen.

Since all the longitudinal stability derivatives of the slender wing are affected[3] similarly by a root gap, the only result derived here is for the lift curve slope. A potential flow solution is sought and the assumptions of slender wing theory are used so that the problem reduces to one of finding a steady velocity potential ϕ that satisfies Laplace's equation and the velocity boundary condition in the cross-flow plane. A system of coordinates is chosen with x and y as shown in Fig. 1. The cross-flow plane at a chordwise station x is shown in Fig. 2a in complex coordinates $y + iz$. The root fence is assumed symmetric with respect to the wing plane. The double slit in the physical ζ plane may be transformed into a single one in the η plane of the form shown in Fig. 2b. The transformation is

$$\frac{d\zeta}{d\eta} = \frac{m^2 - \eta^2}{(p^2 - \eta^2)^{1/2}(\eta^2 - q^2)^{1/2}}$$

where $\zeta = y + iz$, $\eta = Y + iZ$, and the dimensions p, q, m, and d in the η plane are related to g, h, and s in the ζ plane by

$$m = p[E'(k)/K'(k)]^{1/2}, \qquad k = q/p$$

$$g = \pi p/2K'(k)$$

$$h = p\{E'(\tau, k) - (m^2/p^2)F'(\tau, k)\}$$

$$\sin\tau = [(p^2 - m^2)/(p^2 - q^2)]^{1/2}$$

$$s = d\sin\psi - p\{E(\psi, k) - (1 - m^2/p^2)F(\psi, k)\}$$

$$\sin\psi = [(d^2 - p^2)/(d^2 - q^2)]^{1/2}$$

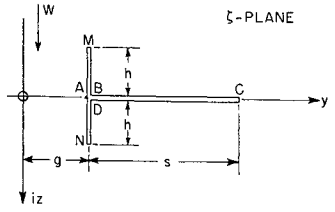

Fig. 2a Physical cross-flow plane.

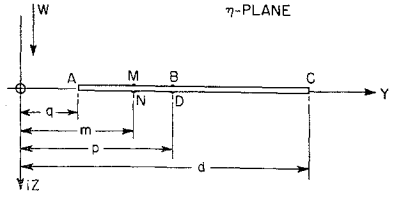

Fig. 2b Transformed cross-flow plane.

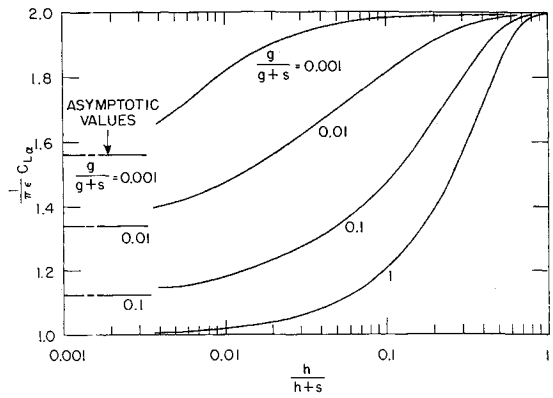

Fig. 3 Variation of lift curve slope with fence height.

Here $E'(k)$, $K'(k)$, $E'(\tau, k)$, $F(\tau, k)$, etc. are elliptic integrals. A solution[4] for the complex potential w which satisfies the velocity boundary conditions at the slit, at the $Y = 0$ plane of symmetry and at infinity, is given by

$$\frac{dw}{d\eta} = \frac{W[\eta^2 - d^2E(k_1)/K(k_1)]}{(d^2 - \eta^2)^{1/2}(\eta^2 - q^2)^{1/2}}$$

where $(1 - k_1^2)^{1/2} = k'_1 = q/d$. Hence on the surface of the wing in the η plane, the velocity potential may be obtained by integration as

$$\phi = -WdZ(\xi, k_1) = -U\alpha dZ(\xi, k_1)$$

where $Z(\xi, k_1)$ is the Jacobian zeta function and the dummy variable ξ is related to the coordinate Y through an elliptic function by $Y = d\,dn\xi$. The cross-flow velocity W for a positive incidence α and freestream flow U is given by $W = U\alpha$.

The lift on the wing and the velocity potential ϕ are related through the pressure coefficient C_p:

$$C_{pu} = -C_{pl} = (2/U)(\partial\phi/\partial x)$$

where the subscripts u and l refer, respectively, to the upper and lower surfaces of the wing.

After integrating the pressure difference chordwise a dummy variable $\sin\theta = sn\xi$ is introduced for the spanwise integration. The upper limit of the integration (corresponding to $y = g + s$) is then denoted by Θ where $\sin\Theta = sn\Xi$ and $dn\Xi = p/d$. Finally the lift is nondimensionalized using the dynamic head and a reference area of a half-wing. To simplify the result a delta wing planform of semi-apex angle ϵ is used (see Fig. 1). The lift curve slope then becomes

$$\frac{1}{\pi\epsilon}C_{L\alpha} = \frac{8}{\pi}\frac{d^2}{s^2}k_1^2 \times \int_0^\Theta \frac{Z(\theta, k_1)\{\sin^2\Theta - \sin^2\theta + (p^2 - m^2)/d^2k_1^2\}\sin\theta}{(1 - k_1^2\sin^2\theta)^{1/2}(\sin^2\Theta - \sin^2\theta)^{1/2}}\,d\theta$$

In Fig. 3 is plotted the lift curve slope as a function of the ratio of fence semiheight to the sum of fence semiheight plus wing semispan. There is a family of curves corresponding to fixed values of the ratio of gap to gap plus semispan. For an infinite root fence height $[h/(h + s) = 1]$, $C_{L\alpha}$ has the value for a full wing without gap, irrespective of the value of $g/(g + s)$. For vanishing fence height the curves asymptote to the values obtained in the references[1–3] previously cited. The results in Fig. 3 indicate that, for large root gaps $[g/(g + s) > 0.1]$, moderate or small fence sizes are not particularly effective. As the gap ratio decreases, a given fence size will give increasing benefit. This is demonstrated in Fig. 4 where a measure of fence effectiveness F_e is plotted against gap ratio for a single value of fence height. The function F_e is defined as

$$F_e = 1 - \{C_{L\alpha}(0) - C_{L\alpha}(0.1, g)\}/\{C_{L\alpha}(0) - C_{L\alpha}(0, g)\}$$

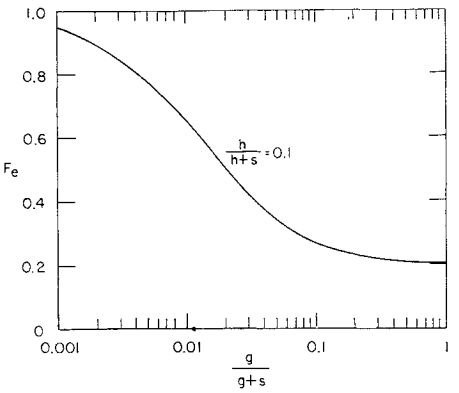

Fig. 4 Fence effectiveness as a function of gap ratio.

where $C_{L\alpha}(0)$ is the lift curve slope for infinite fence (zero gap), $C_{L\alpha}(0.1, g)$ corresponds to the fence height ratio $h/(h + s) = 0.1$ and a given value of $g/(g + s)$, and $C_{L\alpha}(0, g)$ applies to zero fence height but the same value of gap ratio. The closer F_e is to unity the more effective the fence.

Using Fig. 3, a choice can be made of a root fence size that is compatible with the experimental error likely in a particular situation. A minimization of fence dimensions is therefore possible.

References

[1] Bleviss, Z. O. and Strubble, R. A., "Some Aerodynamic Effects of Streamwise Gaps in Low Aspect Ratio Lifting Surfaces at Supersonic Speeds," *Journal of the Aeronautical Sciences*, Vol. 21, No. 10, Oct. 1954, pp. 665–674.

[2] Dugan, D. W. and Hikido, K., "Theoretical Investigation of the Effects upon Lift of a Gap Between Wing and Body of a Slender Wing-Body Combination," TN 3224, 1954, NACA.

[3] Judd, M., "The Effect of a Root Gap on the Aerodynamic Forces of a Slender Delta Wing in Oscillatory Pitching Motion," *The Aeronautical Quarterly*, Vol. XIV, No. 3, Aug. 1963, pp. 299–310.

[4] Glauert, H., *The Elements of Aerofoil and Airscrew Theory*, 2nd ed., Cambridge University Press, Cambridge, England, 1948, p. 173.

Spectroscopically Measured Velocity Profiles of an MPD Arcjet

M.-U. Beth* and M. G. Kling*
Deutsche Forschungs- und Versuchsanstalt für Luft- und Raumfahrt, Institut für Plasmadynamik, Stuttgart-Vaihingen, West Germany

DETAILED comprehension of the physical processes in a plasma jet, for instance the mechanism of acceleration, departures from thermodynamic equilibrium, or dissipation of energy, requires information on spatial resolved plasma parameters. For this purpose, the plasma jet was investigated with respect to the Doppler shift of spectral lines resulting from macroscopic velocities in axial and rotational directions. Certainly many recent papers[1–4] dealt with spectroscopic measurements of arcjet velocities, but to our knowledge no profiles of local velocities were obtained.

Received July 16, 1969. The authors are indebted to P. Tattermusch for useful and active technical assistance.

* Diplomphysiker.

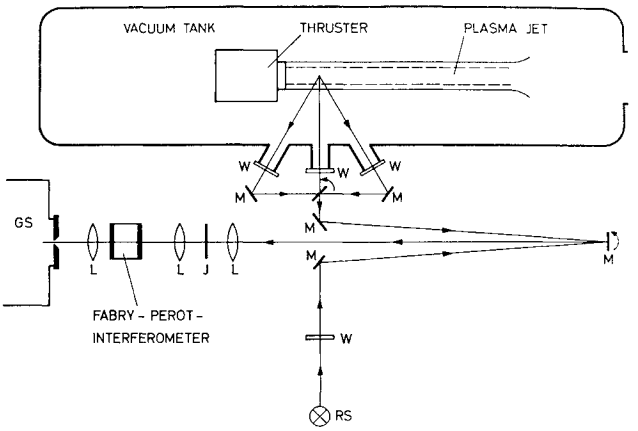

Fig. 1 Optical arrangement, schematic: W = window, M = mirror, RS = radiation standard, L = lens, J = image plane, and GS = grating spectrograph.

The Plasma Jet

The plasma jet was generated by a continuous MPD arc thruster[5] under the following conditions: 650-amps arc current, 40-v arc voltage, 1000-gauss external magnetic field at the cathode tip, 0.22-g/sec argon mass flow, and 0.76-torr background pressure. The off-axis intensity of a spectral line was recorded and observed on an oscilloscope in order to secure reproducibility and no spoke mode operation.

Optical Arrangement

The optical arrangement, see Fig. 1, was chosen in a manner such that the plasma jet was imaged by an achromatic and two telephoto lenses in two steps on the slit (slit width 0.03 cm) of a 2-m plane grating spectrograph. An intermediate image was performed at J, and a Perot-Fabry interferometer of 0.2-cm etalon distance was adjusted between the two telephoto lenses in order to superpose a system of interference fringes on each spectral line. Using this arrangement, both a sufficient spatial and high wavelength-resolution was reached in one dimension, i.e., the slit direction. By interchanging mirrors, optional side-on or angle-on views of the plasma jet could be imaged. Different sections of the latter were observed by displacing the thruster as shown in Fig. 2.

Measurements

Measurements of integrated Doppler shifts along the line of sight originating from plasma rotation have been performed at each section, I, II and III, see Fig. 2, by taking two interferograms with opposite directions of magnetic field and thus changed sense of rotation. The line shifts were obtained photometrically from the photo plate by comparing the distances between homologous fringes in the two interferograms and an exact reproducible marking that was produced by imaging a narrow cross slit with continuous light in each spectrum on the photo plate. (This method differs from that applied in a paper,[6] previously published by the authors, the results of which seem to be doubtful in the light of recent experiments.) The integrated Doppler shifts with respect to

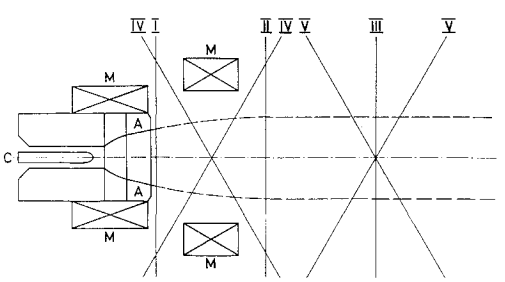

Fig. 2 Thruster and investigated sections, schematic: C = cathode, A = Anode, and M = magnetic coil.